

Effects of the dipolar interaction on the equilibrium morphologies of a single supramolecular magnetic filament in bulk

Pedro A. Sánchez,¹ Joan J. Cerdà,² Tomás Sintés,² and Christian Holm¹

¹*Institute for Computational Physics, Universität Stuttgart. D-70569 Stuttgart, Germany.*^{a)}

²*Instituto de Física Interdisciplinar y Sistemas Complejos, IFISC (CSIC-UIB). Universitat de les Illes Balears. E-07122 Palma de Mallorca, Spain.*^{b)}

We present a study on the equilibrium morphologies of a single supramolecular magnetic filament in a three-dimensional system and their dependence on the effective strength of the magnetic dipolar interactions. The study is based on Langevin dynamics simulations with a bead-spring chain model of freely rotating dipoles. Our results show the existence of three structural regimes as the value of the dipolar coupling parameter is increased: a coil compaction regime, a coil stretching regime and a closed chain regime in which the structures tend progressively to an ideal ring configuration. We also found an indication of the existence of a further regime of closed structures that only can be observed for long enough chains. We discuss in detail the effects governing each regime and the structural transition between open and closed morphologies, as well as the absence of the multiloop configurations found under similar conditions in two-dimensional systems.

I. INTRODUCTION

Supramolecular magnetic filaments are assemblies of nanometer sized magnetic particles linked by polymers or other molecules to form a chain. These systems are the basis of a novel nanotechnology that combines in a unique way the interesting physical properties of magnetic nanoparticles (MNPs) with the intrinsic anisotropies of one-dimensional semi-flexible chains¹.

Research on MNPs has become an extremely active field in recent years^{2–5}. In particular, the self-assembly of MNPs into stable structures, mainly governed by dipolar interactions, is a topic of great interest. The zero-field self-assembly of magnetic colloids into dipolar rings—with the individual magnetic moments disposed in a head-to-tail arrangement along the chain—was predicted more than four decades ago⁶ and since then has been extensively studied by means of theoretical models and simulations^{7–14}. However, the first experimental observations of self-assembled linear chains of MNPs are more recent^{15,16} and, in late years, have led to the finding of different self-assembled structures of two-dimensional dispersions of dipolar chains, including flux closure structures like rings, necklaces or other two-dimensional multiloop configurations^{17–24}. The direct observation of closed ring-like structures in three-dimensional dispersions of MNPs is experimentally challenging, but their existence has been predicted theoretically by means of different simulation models^{20,25–27}.

On the other hand, research on magnetic filaments as a specific system has been more scarce to date. After the seminal works reported in the late 1990s for the assembly of micrometric particles^{28,29}, the progress on their synthesis methods has allowed the preparation of magnetic filaments made of particles of very different materials and

characteristic sizes^{30–37}. In addition, the filaments have increased their degree of flexibility, a property which is mainly determined by the nature of the molecular links between the MNPs and, to some extent, by the intensity of their magnetic interactions. So far, most studies on single or highly diluted magnetic filaments in bulk have been restricted to the understanding of their dynamic properties under the action of external magnetic fields, paying a special attention to their application as nanofluidic propellers and actuators^{22,32,37–43}. The equilibrium configurational properties of the filaments have been generally disregarded. Nevertheless, the chain morphology has been pointed as a relevant factor for some properties of the filaments of high interest like its thermal and electric conductivity or its overall coercivity¹.

As a general hypothesis, it is reasonable to expect that the configurations observed in self-assembled chains of MNPs may appear also as equilibrium morphologies of magnetic filaments with an adequate degree of flexibility. Nevertheless, it is not obvious which conditions may lead to the different equilibrium structures or what will be the behavior of the filaments under conditions which do not lead to the self-assembly of dipolar chains. In addition, there is still little knowledge on the equilibrium structures of highly diluted self-assembled dipolar chains and magnetic filaments in bulk.

In a recent work⁴⁴ we introduced a simple coarse-grained simulation model for the study of the equilibrium behavior of semiflexible magnetic filaments near an attractive flat surface. We reported the effect of the dipolar interactions on the adsorption transition and the existence of different equilibrium morphologies for the adsorbed chain depending on the temperature and the magnetic dipole strength. In agreement with the most recent experimental observations we found different closed chain morphologies on the plane, including rings and two-dimensional multiloop configurations. In the present work we take the same model as a basis to explore the corresponding equilibrium morphologies of magnetic fila-

^{a)}Electronic mail: psanchez@icp.uni-stuttgart.de

^{b)}Electronic mail: joan@ifisc.uib-csic.es

ments in the bulk. In particular, here we intend to qualitatively determine the effects of the magnetic interactions on the local and global configurations of a fully flexible chain without the geometrical constraints imposed by the presence of an adsorbing surface.

The work is organized as follows: in Section II we review the details of the proposed model and the simulation method, in Section III we present and discuss the results of our simulations and we end with the concluding remarks in Section IV.

II. SIMULATION MODEL AND METHOD

In order to explore the equilibrium behavior of a magnetic filament in bulk we have taken just the required ingredients from our previous coarse-grained model⁴⁴: the linking potential, the dipolar interaction and the steric repulsion between the beads. Therefore, in our model a magnetic filament is represented as a bead-spring chain of N identical particles carrying at their centers a point magnetic dipole, $\vec{\mu}$, which can freely rotate in any direction. Since the model does not impose any anisotropy nor explicit probability rates on the reorientation of the dipoles, according to our previous results⁴⁴ we expect a large head-to-tail alignment of the dipoles with respect to the chain backbone for large enough values of the dipolar moment. This head-to-tail arrangement is the natural disposition of chain-like assemblies of ferromagnetic particles in absence of external fields. Nevertheless, this behavior is also found experimentally for chains of superparamagnetic particles as a consequence of a cooperative effect: the increase of the dipole reversal barriers in every bead led by the external field generated by its neighbors⁴⁵. Therefore, we consider that this model might be representative—at least at a qualitative level—for magnetic filaments made either with superparamagnetic or ferromagnetic particles under the conditions that lead to a large head-to-tail alignment of the dipoles.

The details of our model are the following: the steric repulsions between the beads are modeled by means of a Weeks-Chandler-Anderson potential (WCA)⁴⁶:

$$U_{\text{WCA}}(r) = \begin{cases} U_{\text{LJ}}(r) - U_{\text{LJ}}(r_{\text{cut}}), & r < r_{\text{cut}} \\ 0, & r \geq r_{\text{cut}} \end{cases}, \quad (1)$$

where r is the distance between the centers of the interacting beads, $U_{\text{LJ}}(r) = 4\epsilon[(\sigma/r)^{12} - (\sigma/r)^6]$ is the standard Lennard-Jones potential, $r_{\text{cut}} = 2^{1/6}\sigma$ is the shifting parameter selected to make the potential repulsive and σ is the characteristic diameter of the beads. The bonds between adjacent beads in the chain are formed by means of a finite extensible non linear elastic potential (FENE), defined as:

$$U_{\text{FENE}}(r) = \frac{-K_f r_{\text{max}}^2}{2} \ln \left[1 - \left(\frac{r}{r_{\text{max}}} \right)^2 \right], \quad (2)$$

with $K_f = 30/\sigma^2$, and $r_{\text{max}} = 1.5\sigma$. The use of this potential implies to have the linking springs attached to

the center of the beads, therefore neglecting the eventual bond stretching produced by rotations of the linked particles. The long-range magnetic interactions are represented by the conventional point dipole-dipole potential

$$U_{\text{DIP}}(\vec{r}_{ij}; \vec{\mu}_i, \vec{\mu}_j) = \frac{\vec{\mu}_i \cdot \vec{\mu}_j}{|\vec{r}_{ij}|^3} - \frac{3[\vec{\mu}_i \cdot \vec{r}_{ij}][\vec{\mu}_j \cdot \vec{r}_{ij}]}{|\vec{r}_{ij}|^5}, \quad (3)$$

where $\vec{r}_{ij} = \vec{r}_i - \vec{r}_j$ is the displacement vector between the centers of the beads i, j and $\vec{\mu}_i, \vec{\mu}_j$ are the dipole moments associated to each bead. In magnetic dipolar systems it is usual to define a dimensionless dipolar coupling parameter, λ , to represent the effective intensity of the dipolar interactions. For a system of identical dipolar spheres, this parameter is commonly defined as the ratio between the optimum magnetic energy of two dipoles—corresponding to a close contact in a head-to-tail arrangement—over the energy of the thermal fluctuations: $\lambda = \mu_e^2 / (kTb^3)$, where μ_e^2 is the experimental squared dipolar moment of the spheres, k is the Boltzmann constant, T the experimental temperature and b is the characteristic separation distance between the dipoles—typically, the diameter of the beads or, equivalently, the distance between first-nearest neighbors in chain-like systems. We can take reduced units for the experimental parameters by defining $\mu^2 \equiv \mu_e^2 / \epsilon_e$ and $T^* \equiv kT / \epsilon_e$, where ϵ_e is the characteristic experimental strength of the pair interactions in our system. Therefore, we get the following expression for the dipolar coupling parameter:

$$\lambda = \mu^2 / (T^* b^3). \quad (4)$$

This definition suggests that using λ as the leading parameter in a dipolar system makes the variation of μ^2 or T^* basically equivalent from the point of view of the sampling of the parameters space. Nevertheless, one must be aware of the limitations of this equivalence under too extreme conditions. In particular, we expect that for values of λ beyond a characteristic threshold or, equivalently, at very low temperatures, the system behavior will become insensitive to a further increase of this parameter as an indication of the onset of ground state structures. Since our main goal is to determine the effects of the dipolar interactions, we have chosen to sample λ by taking different values of the squared dipolar moment within a moderate range, $\mu^2 \in [0, 20]$, at a constant reduced temperature, $T^* = 1$. However, the dependence of λ on b prevents in our model to sample this parameter in a straightforward way. In particular, we have a bounded but not fixed distance between first-nearest neighbors in the chain. We expect such distance to depend, at least, on either the value of μ^2 and the local degree of head-to-tail alignment of the dipoles. This latter dependence makes the value of b unknown beforehand for any simulation we could attempt, so we can not set λ directly as a running dipolar parameter. On the other hand, it is very convenient to express our results in terms of λ in order to facilitate the comparison with other studies. Our approach

to this issue has been to take μ^2 as the running dipolar parameter of our simulations and, subsequently, to calculate the corresponding values of λ by applying Equation (4), with b being the measured average distance between the first-nearest neighbors in our simulated equilibrium configurations. Finally, for each selected value of the running dipolar parameter, four different chain lengths, $N = \{10, 25, 50, 100\}$, have been sampled.

Our simulations have been performed by means of Langevin dynamics. The translational and rotational Langevin equations of motion for the center of mass of a given bead i and its associated dipole are, respectively:

$$M \frac{d\vec{v}_i}{dt} = \vec{F}_i - \Gamma_T \vec{v}_i + \xi_i^T, \quad (5)$$

$$\vec{I} \cdot \frac{d\vec{\omega}_i}{dt} = \vec{\tau}_i - \Gamma_R \vec{\omega}_i + \xi_i^R, \quad (6)$$

where \vec{F}_i and $\vec{\tau}_i$ are the total applied force and torque, M and \vec{I} the mass and the inertia tensor of the identical particles, Γ_T and Γ_R the translational and rotational friction constants and finally ξ_i^T and ξ_i^R are a zero-mean gaussian random force and torque satisfying the usual fluctuation-dissipation relations. The reduced time t^* is given by $t^* = t\sqrt{\epsilon_e/(M\sigma^2)}$, where t is the measured time. In general, the values of the mass, the inertia tensor and the friction constants are irrelevant for the results associated to an equilibrium state. For simplicity, we have taken $\sigma = 1$, $\epsilon = \epsilon_e = 1$, $M = 1$ and the identity matrix for the inertia tensor in order to ensure isotropic rotations. For the friction constants we have taken $\Gamma_T = 1$, $\Gamma_R = 3/4$, since these values are known to produce a fast relaxation to equilibrium for dipolar systems^{11,12}.

In order to enhance the statistics of the sampling, we have applied the replica exchange molecular dynamics method (REMD)⁴⁷ to our Langevin dynamics simulations by using μ^2 as the replica parameter. For this purpose, we have searched for a minimal set of values of the squared dipolar moment, spanning the desired range $\{\mu_1^2 < \mu_2^2 < \dots < \mu_m^2\} \in [0, 20]$, that would give us exchange rates above 35% for all the replicas and chain lengths. By means of some testing runs we found a set of $m = 66$ unequally spaced values that satisfied such criterium. In summary, the simulation procedure for each tested chain length has been the following: first, we have prepared each replica i by placing in a simulation cell with open boundaries a random chain with its corresponding magnetic dipole of squared moment μ_i^2 associated to each particle. Then, an equilibration cycle of Langevin dynamics with a time step $\delta t = 0.001$ has been run for $3 \cdot 10^6$ steps, enough to ensure that a stationary regime for the total potential energy has been reached at each replica. After this equilibration, we have performed a cycle of $2 \cdot 10^6$ further steps for measurements. Finally, an exchange of the configurations from adjacent replicas has been proposed according the following energy criterium:

$$P_{a \leftrightarrow b} = \min \left(1, e^{-[U_a(\mu_b^2) + U_b(\mu_a^2) - U_a(\mu_a^2) - U_b(\mu_b^2)]} \right), \quad (7)$$

where $U_i(\mu_j^2)$ is the total potential energy of the configuration corresponding to replica i when μ_j^2 is used as the squared dipole moment of the particles. After the exchanges procedure has been finished, a new equilibration cycle using Langevin dynamics has been started. These equilibration-measure-exchange cycles have been repeated until reasonably good statistics has been obtained. REMD simulations should run for enough steps to allow most replicas to complete some round trips through all the values of the exchange parameter. In our case, we checked that 500 equilibration-measures-exchange cycles were enough to allow for no less than four round trips. After such equilibration procedure, we still extended the simulations for 300 more cycles to collect the measures that have been finally used in our statistics.

As a last remark on the simulation method, the limitation of our study to a single filament has made the direct summation the method of choice for the calculation of the long-range dipolar interactions. The simulations have been carried out using the coarse-grained simulation package ESPResSo 3.0.2⁴⁸.

III. RESULTS AND DISCUSSION

In order to present our results in terms of the dipolar coupling parameter, λ , as defined in equation 4, the first property to be determined from the equilibrated filament configurations is the average distance between the first-nearest neighbors, or mean bond length $\langle b \rangle$, as a function of the running dipolar parameter—the squared dipole moment, μ^2 —and the chain length, N . Figure 1 shows the values of $\langle b \rangle$ obtained for every selected chain length along with the corresponding bond length of a dimer—i.e., a chain formed by just two dipoles—which is the minimal conceivable conformation in this system. As one can expect, for all the cases $\langle b \rangle$ decreases smoothly with increasing strength of the dipole moment. On the other hand, the chain length has a significant impact just for the shortest chains at high dipole moments, for which the observed decrease of $\langle b \rangle$ is lower. For longer chains, the change of this $\langle b \rangle$ is almost independent of N . The correct interpretation of this effect requires a detailed analysis of the arrangement of the dipoles in the chain as μ^2 , and consequently λ , are increased. Such discussion is placed in Section III C. Finally, once the dependence of λ on $\langle b \rangle$ has been numerically established for each selected value of μ^2 and N , we can express all our results in terms of λ .

According to previous observations of self-assembled dipolar chains found in ferrofluids and for a semiflexible magnetic filament near an attractive flat surface, it is reasonable to expect either a large disorder in the orientations of the dipoles or a highly ordered head-to-tail arrangement, mainly following the chain backbone, for low and high values of the dipolar coupling parameter, respectively. A direct inspection of the equilibrium morphologies obtained in our simulations confirms this ex-

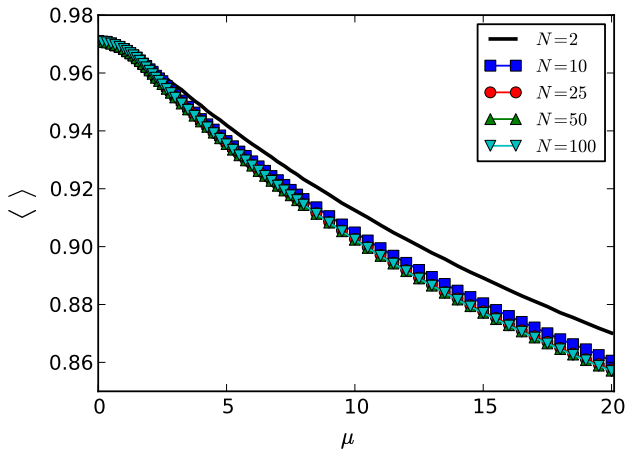


FIG. 1. Mean bond length, $\langle b \rangle$, as a function of the squared dipole moment, μ^2 , for different filament lengths. Error bars are smaller than symbols.

pectation, as well as the existence of important structural changes with the effective intensity of the dipolar interactions. Figure 2 illustrates these changes for some selected values of λ and N . In general, for low values of λ the chains show a shape similar to a swollen random coil, with a high disorder in the orientations of the dipoles. As λ increases, the dipoles tend effectively to align with the chain backbone in a head-to-tail configuration, while the backbone stretches and becomes smoother. At even large values of λ , the chains adopt an irregular ring-like closed structure, with their ends becoming permanently in close contact. Finally, these ringed morphologies tend to reduce their irregularities as λ is further increased. Shorter chains apparently show less backbone irregularities at high values of λ , getting closer to the two-dimensional symmetry of an ideal ring. The rest of Section III is devoted to the formal analysis of these qualitative observations by means of different structural parameters.

A. Characteristic equilibrium structures

The squared radius of gyration, R_g^2 , and end-to-end distance, R_e^2 , are useful parameters for the characterization of the global shape of chain-like structures. Figure 3(a) shows the variation of the scaled mean value of such parameters as a function of λ . Some selected examples of their probability distributions are also shown in Figures 3(b) and 3(c). Two cases of the theoretical scaling relation $\langle R_g^2 \rangle \propto N^{2\nu}$ have been assumed for the representation of the data in Figure 3(a): the upper and middle panels show the values of $\langle R_e^2 \rangle$ and $\langle R_g^2 \rangle$ scaled with the exponent $2\nu = 6/5$. This exponent corresponds to an ideal self-avoiding walk, which is the expected behavior for this system in the limit $\lambda \rightarrow 0$. The lower panel of Figure 3(a) shows $\langle R_g^2 \rangle$ scaled with the exponent $2\nu = 2$, that corresponds to the ideal structure that we expect

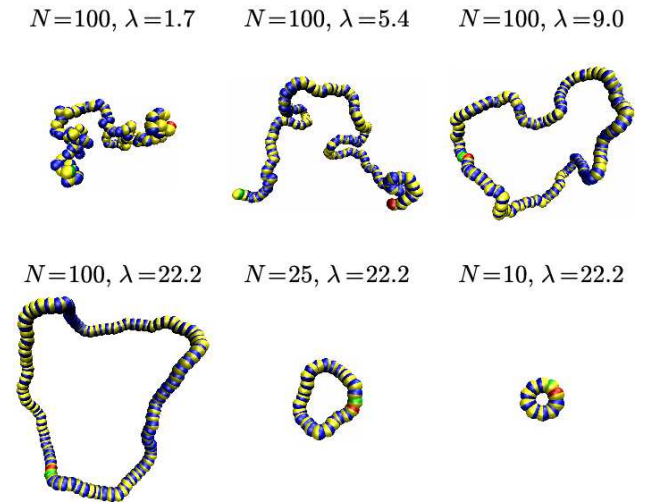


FIG. 2. Selected snapshots of equilibrium configurations obtained for different values of the dipolar coupling parameter, λ , and chain lengths, N . The magnetic beads are represented as two-color spheres, with colors indicating the orientation of the associated dipole.

for $\lambda \gg 1$: the perfect ring. We can observe that the curves tend to collapse at different regions according to each scaling behavior: low values of λ for $2\nu = 6/5$ and large values of λ for $2\nu = 2$. However, it is remarkable that a perfect collapse has not been reached in any case. This result indicates that the system is far from an ideal behavior, specially for the limit of large values of λ .

Independently of the scaling applied to the data, the results shown in Figure 3 clearly indicate the existence of three different regimes and a transition-like structural change within the explored range of parameters: for $\lambda \lesssim 2$ the chain structures tend to compact slightly with λ , an effect that increases with the chain length. For $2 \lesssim \lambda \lesssim 7$ this tendency is reversed, with a remarkable stretching of the structures until a maximum of the overall extension is reached. This maximum is absolute for the end-to-end distance in all the cases. Instead, for the radius of gyration this maximum is just relative except for the shortest chains. At $\lambda \sim 7$ the chain overall extension experiences a sudden drop, with the end-to-end distance falling to its minimum equilibrium value, corresponding to the close contact separation between two non-bonded, head-to-tail oriented particles. In addition, the corresponding probability distributions show the existence of notably bigger fluctuations of both structural parameters in this region. This important change corresponds to the structural closure transition that leads to the ring-like morphologies pointed out above. Finally, for $\lambda \gtrsim 7$ the end-to-end distance remains in its minimum value, showing almost a delta function in its probability distribution, and the radius of gyration tends monotonically to a plateau. The value of this plateau is slightly lower than the corresponding to an ideal ring formed by N beads of effective diame-

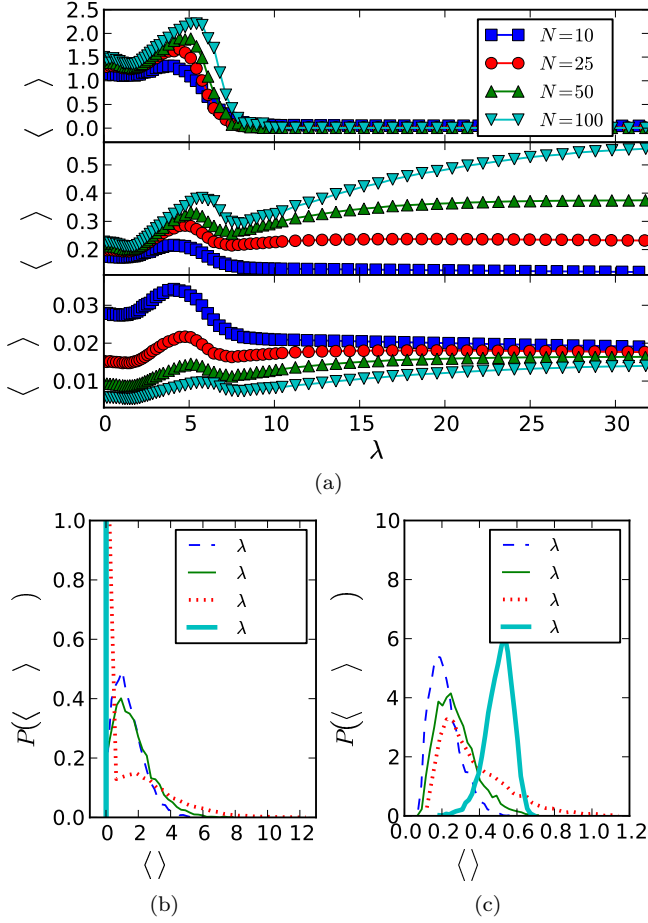


FIG. 3. (a) Scaled mean squared value of the end-to-end distance (upper panel) and radius of gyration (middle and lower panels), as a function of the dipolar coupling parameter, λ , for different chain lengths. The scaling shown in the upper and middle panels corresponds to the behavior expected for a self-avoiding walk, $\langle R_g^2 \rangle \propto N^{6/5}$. The scaling in the lower panel corresponds to the ideal ring behavior, $\langle R_g^2 \rangle \propto N^2$. (b) Probability histograms of $\langle R_g^2 \rangle / N^{6/5}$ obtained for $N = 100$ and some selected values of λ . (c) Corresponding probability histograms for $\langle R_g^2 \rangle / N^{6/5}$.

ter b , $R_{g, ring}^2 = b^2 / [4 \sin^2(\pi/N)] \sim [Nb / (2\pi)]^2$. It is also remarkable that the tendency to the plateau and its similarity to the value expected for an ideal ring are significantly lower for the longest chains. As an example, for $N = 10$ and $\lambda \approx 30.39$ the mean squared radius of gyration measured for our equilibrium structures is $\langle R_g^2 \rangle \approx 1.92$, while an equivalent ideal ring would have $R_{g, ring}^2 \approx 1.95$. On the other hand, for $N = 100$ and $\lambda \approx 30.79$ we have measured $\langle R_g^2 \rangle \approx 139.25$ in front of the ideal value $R_{g, ring}^2 \approx 186.88$. Therefore, the difference between the measured and the ideal values for R_g^2 at $\lambda \sim 30$ is of the order of 10% for $N = 10$ and 25% for $N = 100$. This effect will be better illustrated in Section III C.

The strong dependence of the closed structures with

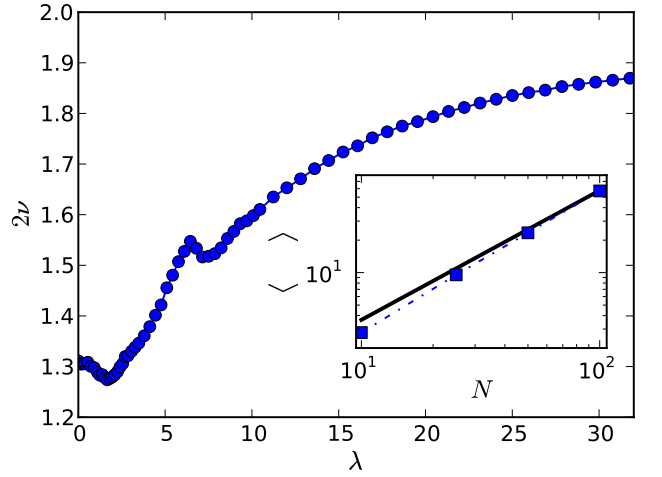


FIG. 4. Dependence with λ of the fitted exponent, 2ν , corresponding to the scaling relation for the squared radius of gyration $\langle R_g^2 \rangle \propto N^{2\nu}$ (main plot). The inset shows how the values of $\langle R_g^2 \rangle$ measured for $\lambda = 0$ (data points) deviate from the ideal scaling, given by $2\nu = 6/5$ (solid line).

the chain length discussed above explains the deviation with respect to the ideal scaling behavior for large values of λ that has been observed in Figure 3(a). The deviation corresponding to small values of λ is instead a consequence of sampling too short chains. This effect can be evidenced by fitting the scaling exponent 2ν to the available data. In Figure 4 we have represented the fitted exponent as a function of the dipolar coupling parameter. The fit has been performed by using all the simulated chain lengths. The result is qualitatively consistent with the theoretical expectations: we can observe that the value of 2ν is effectively bounded by the values corresponding to the Flory exponent for the three-dimensional swollen random coil, $2\nu = 6/5$, and the ideal ring, $2\nu = 2$. The local peak observed at $\lambda \sim 6$ corresponds to the maximum stretching of the chain prior to the closure transition. However, the inset of Figure 4 evidences that the exponent fitted for $\lambda = 0$ is slightly higher than the theoretical value due to the fact that we have not reached the asymptotic scaling regime in our sampling. An accurate estimation of the scaling exponent for the limit $\lambda \rightarrow 0$ would require the simulation of longer chains.

Another general effect of the dipolar interactions on the chains is to locally stretch the backbone as λ is increased, apparently in a rather independent way with respect to the global structure. This magnetically driven local bond stretching has a similar effect than the chain stiffness associated to bond bending potentials⁴⁴. Nevertheless, it is important to keep in mind that the non-local structural effects of the dipolar interactions and the bond stiffness are completely different. In other chain-like systems governed by long-ranged interactions—like, for example, in polyelectrolyte systems—the effects of the intensity of such interactions on the local structure

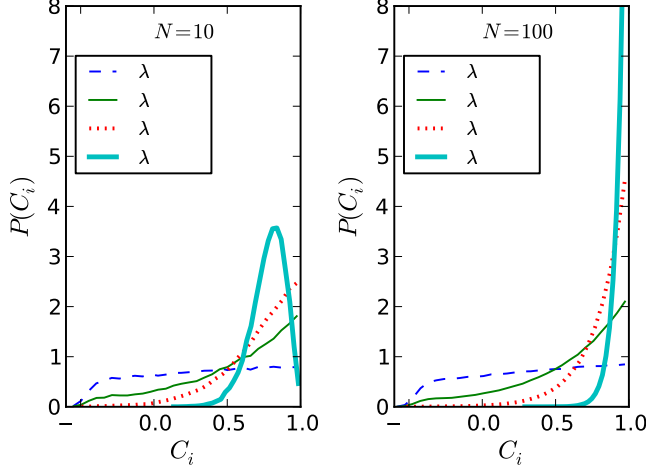


FIG. 5. Probability distributions of the cosinus bond angle parameter corresponding to $N = 10$ (left) and $N = 100$ (right) obtained for different values of the dipolar coupling parameter.

of the chain are usually studied by means of the persistence length^{49,50}. In our case, however, the existence of a closure transition led by the intra-chain long-ranged dipolar interactions introduces a non-local dependence of this parameter (for a discussion on the locality of the persistence length see for instance ref.⁵¹ and references therein). Therefore, we choose to analyze a simple but representative local parameter: the cosine bond angle distribution. This is defined as the probability distribution of the vector product of adjacent unitary bond vectors for every position i along the chain:

$$C_i = \hat{b}_{i-1,i} \cdot \hat{b}_{i,i+1}, \quad (8)$$

where $\hat{b}_{i,j}$ is the unitary vector pointing in the direction from the center of bead i to the center of bead j . Figure 5 shows the distributions for the cases $N = \{10, 100\}$ corresponding to some selected values of the dipolar coupling parameter. The results show a continuous change with λ from an almost flat distribution, with a wide domain of values for C_i , to a distribution that progressively approaches a delta function at the point corresponding to an ideal ring:

$$C_i(\lambda \gg 1) \rightarrow \delta[\cos(2\pi/N)]. \quad (9)$$

The almost flat distribution observed at low values of λ indicates an insignificant correlation between adjacent bond vectors. For high values of λ the adjacent bond vectors are highly correlated, as this corresponds to a locally stretched backbone. In all cases C_i is unable to take values far below -0.5 as a direct consequence of the steric repulsions.

In Sections III B and III C we analyze in more detail the structural properties found for low and high values of λ , respectively.

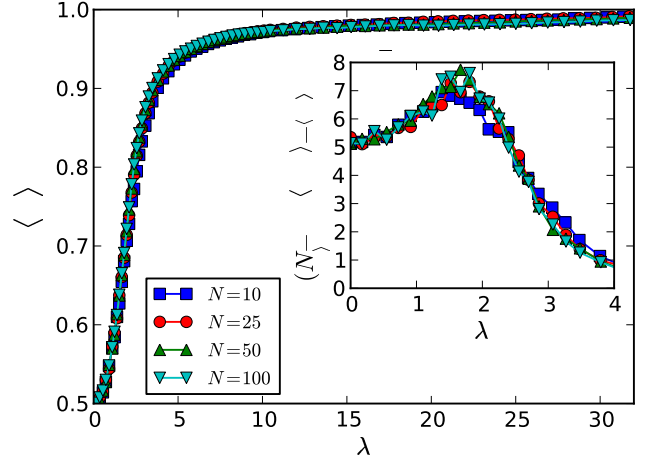


FIG. 6. Average bond-dipole alignment modulus, $\langle A \rangle$, as a function of the dipolar coupling parameter for different chain lengths. Its corresponding fluctuations for low values of λ , scaled according to the sampling statistics, are shown in the inset.

B. Properties of open structures

We have shown that two different regimes are found for open structures. In order to understand this behavior, we have analyzed in the first place the degree of alignment of the dipoles with the chain backbone. This alignment can be easily calculated by means of the bond-dipole alignment modulus, A , defined as⁴⁴:

$$A = \frac{1}{N-2} \sum_{i=2}^{N-1} \left| \hat{b}_{i-1,i+1} \cdot \hat{\mu}_i \right|, \quad (10)$$

where $\hat{\mu}_i$ is a unit vector parallel to the dipolar moment of bead i and $\hat{b}_{i-1,i+1}$ is again a unit vector parallel to the displacement vector between the centers of the beads $i-1$ and $i+1$. We expect that for any given equilibrium configuration found in our system this simple parameter will take values from 1/2 to 1. The value 1/2 will correspond to a distribution of dipole orientations completely uncorrelated with the chain backbone and the value 1 to a configuration with all dipoles perfectly aligned with it. Figure 6 shows the average and fluctuations of this parameter as a function of λ for every chain length: a transition-like behavior for $\langle A \rangle$ around $\lambda \sim 1.5$ can be observed, with a relatively abrupt jump from the fully uncorrelated state into a highly correlated one and a very weak dependence on the chain length. For high values of λ , the parameter is observed to remain monotonically approaching 1. Interestingly, the maxima in the fluctuations of the transition-like jump corresponds quite well with the minima found for R_g^2 and R_e^2 that separates the two behaviors associated to open structures. Furthermore, the value of λ at which the ordering transition seems to take place agrees quite well with the value known as the condition for the self-assembly of spheric MNPs into dipolar head-to-tail chains, $\lambda > 2^{6,16,52}$. The

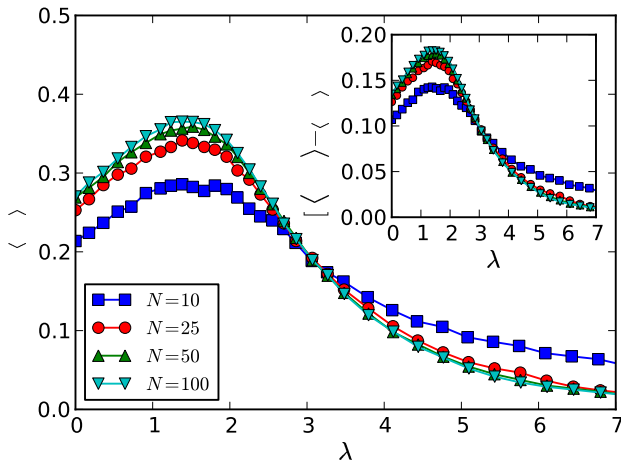


FIG. 7. Relative average number of correlated lateral contacts, $\langle n_c \rangle/N$, for low values of λ and different chain lengths. Inset shows the corresponding fluctuations. See the text for a definition of $\langle n_c \rangle$.

self-assembly into head-to-tail conformations should be possible only if the thermal fluctuations are less significant than the magnetic energy of two perfectly aligned dipoles. Several previous studies on the self-assembly of dipolar particles have reported a negligible probability of particle aggregation for values of the dipolar coupling parameter strictly below $\lambda < 2$, neither into head-to-tail chain-like structures nor into three-dimensional clusters of correlated dipoles^{52–55}. However, it should be noted that there exists at least one favoring factor in the dipole ordering that is absent in the self-assembly of freely interacting dipolar particles: in our system, the chain connectivity and the close contact between neighbor dipoles is guaranteed independently of the thermal fluctuations. In particular, in our model the bond length is not fixed but is strictly bounded to a short distance, thus the presence of the bonds reduces the degrees of freedom of the dipoles and, consequently, their configurational entropy, an effect that should favor the local alignment of the dipoles.

According to the previous observations, we conclude that a compaction or a stretching of the open chains is obtained depending on the degree of alignment of the dipoles with the chain backbone. In particular, disordered dipoles tend to favor the chain compaction by increasing their lateral contacts and allowing the formation of small, weakly interacting, three-dimensional clusters that reduce the overall extension of the chain. The monotonous decrease of the bond length with λ may help slightly to the overall compaction in this region, but its impact can be neglected in front of the variations of the lateral contacts. These variations can be measured by means of a careful count that should include dipole correlations and energy criteria in order to exclude as far as possible the pure thermal fluctuations effects. Therefore, we defined the average number of lateral contacts, $\langle n_c \rangle$, as the average number of bead pairs, $\{i, j\}$, that satisfy

the following criteria: first, we exclude from the count the first-nearest neighbors, $|i - j| \neq 1$, and the particles at the chain ends, $i, j \neq \{1, N\}$; second, the particles should be in “close contact”, thus their separation distance should be lower than the maximum extension of a bond, $\|\vec{r}_{ij}\| < 1.5\sigma$; third, the absolute value of the normalized scalar product of their respective dipolar moments should be bigger than the corresponding to a random distribution of dipole orientations, $|\vec{\mu}_i \cdot \vec{\mu}_j| > 0.5$; finally, the pair magnetic energy of the particles should be strictly negative, $U_{\text{DIP}}(\vec{r}_{ij}; \vec{\mu}_i, \vec{\mu}_j) < 0$. The combination of these conditions, which are similar to the energy and entropy criteria established for the aggregation of magnetic particles in ferrofluids⁵⁶, ensure that the corresponding lateral contacts are most likely to be driven by attractive dipolar interactions. Figure 7 shows the relative values of this parameter measured for each chain length at the region of low values of λ . As we expected, $\langle n_c \rangle$ increases with the dipolar parameter up to a maximum at around $\lambda \sim 1.5$, which is the dipole ordering point that separates the compaction and the stretching regimes, and finally decreases for higher values of λ . It can also be noted that longer chains tend to have slightly more average lateral contacts, leading to a more pronounced compaction regime, in agreement with the behavior observed in Figure 3.

C. Closure transition and properties of closed structures

The inspection of the configurations and the behavior of the radius of gyration and the end-to-end distance has evidenced the existence of a closure transition in our model. It is known that the dipolar energy of a chain of $N > 4$ dipoles arranged into a head-to-tail closed ring is lower than the corresponding to a head-to-tail stretched arrangement of the same length⁵⁷. In particular, for $N > 4$, the decrease of the dipolar energy led by the added head-to-tail close contact between the chain ends overcomes the effect of the local misalignment introduced by the ring curvature. On the other hand, a closed chain structure has a lower configurational entropy than a open one. Therefore, the closure transition separates the region of configurations controlled by entropy, corresponding to the open chain structures, from the energy-controlled region of closed structures.

In order to analyze in more detail the closure transition of our equilibrium structures, we chose the total magnetization of the chain as the characteristic parameter. This is simply defined as the module of the vector sum of the unitary dipolar moments along the chain:

$$M = \left\| \sum_{i=1}^N \hat{\mu}_i \right\|. \quad (11)$$

The behavior of this parameter is expected to be qualitatively very similar to the observed for the end-to-end distance⁴⁴, but has an additional advantage over the lat-

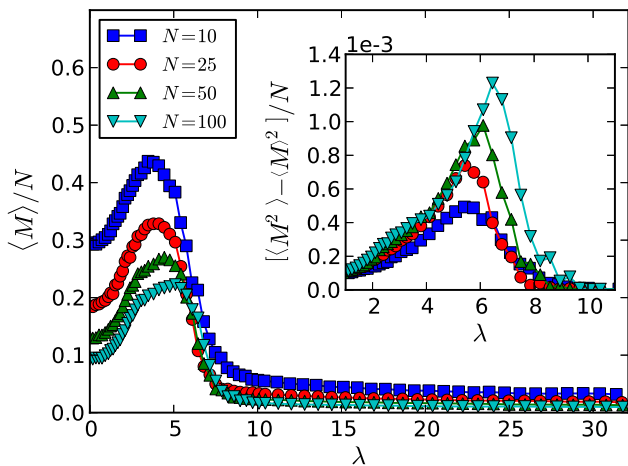


FIG. 8. Mean total magnetization as a function of the dipolar coupling parameter for different chain lengths and its corresponding fluctuations (inset).

ter: since the domain of values sampled by M is considerably smaller than the corresponding to R_e^2 , it is far easier to obtain accurate statistics for the fluctuations of M . Figure 8 represents the relative mean value of this parameter and its fluctuations. As expected, its behavior for $\lambda > 2$ is analogous to what has been observed for R_e^2 : it grows with λ up to a maximum, from which a sudden drop to almost zero is found around $\lambda \sim 7$. Finally, for high values of λ it remains close to zero. This almost zero value of M indicates that the magnetic flux along the chain is following a nearly closed trajectory, as corresponds to a closed structure of head-to-tail aligned dipoles. Remarkably, the fluctuations of M , shown in the inset of Figure 8, display very clear peaks indicating the transition points, λ_0 , which move slightly towards higher values of the dipolar coupling parameter as the chain length increases: from $\lambda_0 \sim 5.5$ for $N = 10$ to $\lambda_0 \sim 6.5$ for $N = 100$. These closure points are consistent with the structural phase diagram known for dispersions of free MNPs⁵⁸. In particular, ring-like closed structures are found for values of λ higher than the self-assembly condition, $\lambda \gtrsim 2.5$, at low dispersion densities. Our results indicate that there exist an important difference in the flux closure behavior of free MNPs and magnetic filaments. In particular, we have shown that in our model all the filaments remain persistently in a closed arrangement for values of λ higher than the transition point. However, it is well known that self-assembled structures of free MNPs tend to be quite heterogeneous, with a coexistence of open and closed structures in a wide range of parameters. This coexistence is not limited to experimental observations—in which other more complex short ranged interactions, hard to control and predict, might play an important role in the self-assembly process—but is also found in simulations with other minimalistic models similar to ours. To our best knowledge, an abrupt closure transition in self-assembled structures of free MNPs, lead

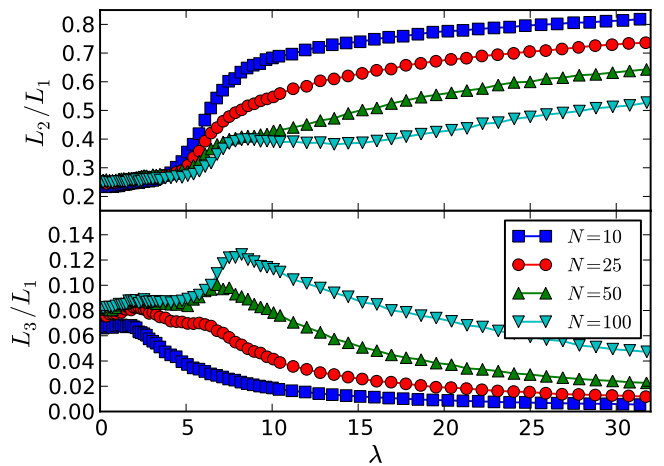


FIG. 9. Shape parameters of the chains for every sampled value of λ and N . These shape parameters are defined as the ratios of the average principal moments of the gyration tensor: L_2/L_1 (upper panel) and L_3/L_1 (lower panel).

by a change in λ in absence of external fields, has never been observed and is not expected to exist due to the inherent polydispersity of such self-assemblies. This suggests that magnetic filaments with defined lengths might have a more coherent and controllable experimental equilibrium behavior than directly self-assembled structures of MNPs, thus they might facilitate the synthesis of more complex magnetic nanostructures.

We have seen that in all the cases the chains remain in a closed configuration for $\lambda > \lambda_0$, but we need to determine how far are these closed structures from an ideal ring configuration. The closeness of the chain structures to specific ideal configurations can be characterized by means of different shape parameters calculated from the average principal moments of the gyration tensor of the sampled configurations, $L_1 \geq L_2 \geq L_3$. Here we choose to analyze the ratios of the average second and third moments to the first one, L_2/L_1 and L_3/L_1 respectively. Figure 9 shows the behavior of these parameters with λ for every chain length. For $\lambda = 0$ we can observe that our measures are in good agreement with the ratios corresponding to the shape anisotropy of a swollen random coil, $L_1 : L_2 : L_3 \approx 12 : 3 : 1$ ⁵⁹. For $\lambda > 0$ these shape parameters provide more insights on the structures of the different regimes. In the coil compaction region ($\lambda \lesssim 2$) there is a very small increase of both ratios, L_2/L_1 and L_3/L_1 , which can be observed for all the chain lengths and that corresponds to an slightly enhanced structural isotropy led by the lateral contacts. Most of the coil stretching region ($2 \lesssim \lambda \lesssim 5$) is characterized by a decrease in L_3/L_1 corresponding to the increased shape anisotropy that is expected from the local stretching of the chain. However, this effect becomes less evident as the chain length increases and L_2/L_1 seems to remain almost constant. In order to understand this behavior, one should take into account that in this region the fluc-

tuations of the global structure grow with λ , as we have shown in Figures 3(c) and 3(b), as well as with N . Since the fluctuations make the chains to sample a wider region of the configurational space, they tend to hinder the effects of the local stretching on the average values of the moments. The impact of the structural fluctuations and its dependence on the chain length become even more evident in the region of the closure transition ($5 \lesssim \lambda \lesssim 8$). In this case we can observe a significant increase of the isotropy with respect to the two first principal axes, as evidences L_2/L_1 , specially for the shorter chains. The dependence of the third dimension on the chain length is instead the opposite: as the chain length increases, a more pronounced increase of the isotropy with respect to the third principal axis can be observed. As shows L_3/L_1 , the closed chains found persistently for $\lambda > 8$ are relatively flat structures that tend to be closer to a two-dimensional ring as λ increases. Nevertheless, L_2/L_1 evidences that these rings are quite asymmetric, having the shape of an irregular ellipse. It is known that semiflexible closed chains tend to show elliptical shapes rather than a symmetric, circular one⁶⁰. More interestingly, the behavior of L_2/L_1 suggests the existence of a further structural regime of closed morphologies, for values of λ just above of the closure region, that might be only observed for long enough chains. In particular, the curve corresponding to $N = 100$ indicates that the two-dimensional anisotropy of the closed structures is growing slightly with λ within the region $8 \lesssim \lambda \lesssim 14$. However, to test this hypothesis further simulations with longer chains are needed.

In our simulations, we found no trace of two-dimensional multiloop structures in equilibrium. This result differs from the experimental observation in assemblies of MNPs in quasi two-dimensional systems^{17–19,21,22,24} and the theoretical predictions of magnetic filaments adsorbed onto a planar surface⁴⁴. Smooth two-dimensional multiloop structures can be slightly more energetically favorable than a single ideal ring, provided they keep the closed head-to-tail contact between the chain ends and add some favorable lateral contacts. On the other hand, the formation of such lateral contacts between middle points in the chain induces a decrease in the configurational entropy with respect to a single ring. The balance between the changes in the configurational energy and entropy associated to the formation of multiloop structures depends on the system dimensionality: the presence of a steric or adsorbing surface imposes a two-dimensional arrangement of the chains, leading to a significant decrease in their configurational degrees of freedom. Due to this entropy reduction mechanism, the formation of multiloop chains requires a smaller change of entropy in two-dimensional systems than in the bulk, thus it is favoured in a broad range of parameters. Nevertheless, we expect that multiloop configurations will be observed in bulk for low enough temperatures, when energetic contributions overcome the entropic ones.

At the beginning of Section III we provided an evi-

dence of the significant impact of the chain length on the mean bond length, $\langle b \rangle$, for short chains and strong dipolar interactions (see Figure 1). Instead, the variation of $\langle b \rangle$ with λ is practically indistinguishable for long chains. On the other hand, we have evidenced that for large values of λ the dipoles show a high degree of head-to-tail alignment with the chain backbone which is independent of N (Figure 6). Therefore, an important contribution to the dependence of the bond length with N for short chains should correspond to the behavior of the cosine bond angle distribution and its upper bound limit for $\lambda \gg 1$, defined in Equation (9). As a consequence, shorter chains have a higher degree of misalignment even for the case of an ideal ring structure. In other words, the closed structure imposes a higher local curvature on the chain backbone for the shorter chains, which leads to an increased misalignment of the dipoles. Nevertheless, the case $N = 2$ shown in Figure 1 evidences that the misalignment between first-nearest neighbors led by the local curvature is not enough to fully characterize the complex dependence of $\langle b \rangle$ on N . Obviously, a system of two dipoles is not a closed structure and has no defined curvature. In fact, for high values of λ , this system remains as a minimal rod with both dipoles in a highly aligned head-to-tail orientation. All these observations suggest consistently that there is a significant effect of the dipoles beyond the range of the first-nearest neighbors on the bond length and, consequently, on the values of λ that characterize each structural region and the closure transition.

IV. CONCLUDING REMARKS

We have studied the equilibrium behavior of a single, fully flexible supramolecular magnetic filament under the influence of long ranged dipolar interactions between their constituent MNPs, and the anisotropies and entropic effects associated to the chain-like structure. The study has been carried out by means of Langevin dynamics simulations with a bead-spring model of linked but otherwise freely rotating dipoles.

By increasing the effective strength of the dipolar interactions at a constant temperature, we observed that the dipoles tend to increase their alignment with the chain backbone in a head-to-tail arrangement, favoring the formation of locally stretched structures and leading to an increase of the orientational correlations between dipoles that are spatially close in the chain sequence. These local effects are observed together with important changes in the overall morphology of the chains that allow to clearly distinguish three different structural regions. For low values of the dipolar coupling parameter the filament structure is similar to the corresponding to a three-dimensional swollen random coil, displaying a transition-like behavior from an initial compaction towards a stretching process that is associated to the change in the degree of the local alignment of

the dipoles with the chain backbone. The compaction region is characterized by the formation of small clusters of dipoles that establish favorable lateral contacts. The stretching region appears at the characteristic point of the transition-like alignment of the dipoles with the backbone, which approximately corresponds to the condition of self-assembly of free MNPs into stable clusters, $\lambda \sim 2$. At around $\lambda \sim 7$ the dipoles show already a high degree of alignment with the backbone and the chain experiences a closure transition, signaling the onset of energy-controlled closed configurations that consist in irregular elliptic ring-like structures. In general, as the dipolar coupling parameter is further increased, such irregular closed structures tend to approach the morphology of an ideal ring. However, we found an indication of the existence of a further intermediate structural region, observed within a range of values of λ just above the closure transition, in which the rings formed by long enough chains would tend towards a more eccentric elliptic structure.

Our results also evidence the impact of the chain length on its structural behavior. In general, this impact can be considered a complex manifestation of the strong dependence of the conformational entropy on the chain length. These length-dependent entropic effects may affect significantly the values of the dipolar coupling parameter that characterize each structural region and, particularly, the closure transition. In addition we have shown that, as long as some flexibility is allowed for the links between particles, the long-range contributions beyond the range of the nearest neighbor ones can significantly modify the estimation of the average bond length and, with it, the effective strength of the dipolar interactions in the system.

We discussed the absence of equilibrium multiloop configurations in our three-dimensional system analogous to the ones found theoretically and experimentally in two-dimensional systems. We think that the main reason for this absence is the importance of entropic effects in the three-dimensional system that prevent the formation of such multiloop configurations, but we still expect it to appear in bulk for low enough temperatures. The strong dependence of the entropy on the chain length and the evident inadequacy of the usual estimation of the effective dipolar strength at very low temperatures suggest that the characterization of the multiloop regimes might be a rather challenging task.

As a last remark, despite complex interplay between energy and entropy, all our results indicate the existence of well defined structural regimes, in difference to what is observed in the self-assembly of free MNPs. This suggests that magnetic filaments can be more adequate building blocks for the synthesis of complex magnetic nanostructures.

ACKNOWLEDGEMENTS

We thank Peter Košován for useful discussions. We also thank the following projects for the computational resources: bwGRiD⁶¹, GRID-CSIC⁶² and FISICOS (FIS2007-60327, funded by the Spanish MICNN and the ERDF).

- ¹H. Wang, Y. Yu, Y. Sun, and Q. Chen, *Nano* **06**, 1 (2011).
- ²R. Kodama, *J Magn Magn Mater* **200**, 359 (1999).
- ³S. P. Gubin, Y. A. Koksharov, G. B. Khomutov, and G. Y. Yurkov, *Russ Chem Rev* **74**, 489 (2005).
- ⁴S. A. Majetich and M. Sachan, *J Phys D Appl Phys* **39**, R407 (2006).
- ⁵S. Mørup, M. Hansen, and C. Frandsen, in *Comprehensive Nanoscience and Technology*, edited by D. L. Andrews, G. D. Scholes, and G. P. Wiederrecht (Academic Press, Amsterdam, 2011) Chap. 1.14, pp. 437–491.
- ⁶P. de Gennes and P. Pincus, *Zeitschrift für Physik B Condensed Matter* **11**, 189 (1970).
- ⁷M. A. Osipov, P. I. C. Teixeira, and M. M. Telodagama, *Phys Rev E* **54**, 2597 (1996).
- ⁸H. Morimoto, T. Maekawa, and Y. Matsumoto, *Phys Rev E* **68**, 061505 (2003).
- ⁹K. Morozov and M. Shliomis, in *Ferrofluids*, Lecture Notes in Physics, Vol. 594, edited by S. Odenbach (Springer Berlin Heidelberg, 2003) pp. 162–184.
- ¹⁰K. I. Morozov and M. I. Shliomis, *J Phys-Condens Mat* **16**, 3807 (2004).
- ¹¹J. J. Cerdà, S. Kantorovich, and C. Holm, *J Phys-Condens Mat* **20**, 204125 (2008).
- ¹²S. Kantorovich, J. J. Cerdà, and C. Holm, *Phys Chem Chem Phys* **10**, 1883 (2008).
- ¹³T. Prokopyeva, V. Danilov, S. Kantorovich, and C. Holm, *Phys Rev E* **80**, 031404 (2009).
- ¹⁴T. Prokopyeva, V. Danilov, A. Dobroserdova, S. Kantorovich, and C. Holm, *J Magn Magn Mater* **323**, 1298 (2011).
- ¹⁵K. Butter, P. H. H. Bomans, P. M. Frederik, G. J. Vroege, and A. P. Philipse, *Nature Materials* **2**, 88 (2003).
- ¹⁶M. Klokkenburg, C. Vonk, E. M. Claesson, J. D. Meeldijk, B. H. Erne, and A. P. Philipse, *J Am Chem Soc* **126**, 16706 (2004).
- ¹⁷S. L. Tripp, R. E. Dunin-Borkowski, and A. Wei, *Angew Chem Int Edit* **42**, 5591 (2003).
- ¹⁸Y. Xiong, J. Ye, X. Gu, and Q.-w. Chen, *J Phys Chem C* **111**, 6998 (2007).
- ¹⁹H. Wang, Q.-W. Chen, Y.-B. Sun, M.-S. Wang, L.-X. Sun, and W.-S. Yan, *Langmuir* **26**, 5957 (2010).
- ²⁰M. Yoon and D. Tománek, *J Phys-Condens Mat* **22**, 455105 (2010).
- ²¹A. Wei, T. Kasama, and R. E. Dunin-Borkowski, *J Mater Chem* **21**, 16686 (2011).
- ²²J. J. Benkoski, J. L. Breidenich, O. M. Uy, A. T. Hayes, R. M. Deacon, H. B. Land, J. M. Spicer, P. Y. Keng, and J. Pyun, *J Mater Chem* **21**, 7314 (2011).
- ²³W.-F. Ding, Z. Li, H. Zhou, B. Zhao, J.-g. Wan, F. Song, and G.-H. Wang, *J Phys Chem C* **116**, 10805 (2012).
- ²⁴M. W. Szyndler and R. M. Corn, *J Phys Chem Lett* **3**, 2320 (2012).
- ²⁵A. Satoh, R. W. Chantrell, S.-I. Kamiyama, and G. N. Coverdale, *J Colloid Interface Sci* **181**, 422 (1996).
- ²⁶M. Aoshima and A. Satoh, *J Colloid Interface Sci* **280**, 83 (2004).
- ²⁷L. Rovigatti, J. Russo, and F. Sciortino, *Soft Matter* **8**, 6310 (2012).
- ²⁸E. M. Furst, C. Suzuki, M. Fermigier, and A. P. Gast, *Langmuir* **14**, 7334 (1998).
- ²⁹E. M. Furst and A. P. Gast, *Phys Rev Lett* **82**, 4130 (1999).
- ³⁰R. Dreyfus, J. Baudry, M. L. Roper, M. Fermigier, H. A. Stone, and J. Bibette, *Nature* **437**, 862 (2005).

- ³¹O. Tabata, H. Kojima, T. Kasatani, Y. Isono, and R. Yoshida, in *Proceedings IEEE Sixteenth Annual International Conference on Micro Electro Mechanical Systems* (2003) pp. 12–15.
- ³²B. A. Evans, A. R. Shields, R. L. Carroll, S. Washburn, M. R. Falvo, and R. Superfine, *Nano Lett* **7**, 1428 (2007).
- ³³P. Y. Keng, I. Shim, B. D. Korth, J. F. Douglas, and J. Pyun, *ACS Nano* **1**, 279 (2007).
- ³⁴S. E. Bowles, W. Wu, T. Kowalewski, M. C. Schalnatz, R. J. Davis, J. E. Pemberton, I. Shim, B. D. Korth, and J. Pyun, *J Am Chem Soc* **129**, 8694 (2007).
- ³⁵J. J. Benkoski, S. E. Bowles, R. L. Jones, J. F. Douglas, J. Pyun, and A. Karim, *J Polym Sci, Part B: Polym Phys* **46**, 2267 (2008).
- ³⁶Z. Zhou, G. Liu, and D. Han, *ACS Nano* **3**, 165 (2009).
- ³⁷J. J. Benkoski, R. M. Deacon, H. B. Land, L. M. Baird, J. L. Breidenich, R. Srinivasan, G. V. Clatterbaugh, P. Y. Keng, and J. Pyun, *Soft Matter* **6**, 602 (2010).
- ³⁸A. Čēbers, *Curr Opin Colloid Interface Sci* **10**, 167 (2005).
- ³⁹M. Belovs and A. Čēbers, *Phys Rev E* **79**, 051503 (2009).
- ⁴⁰F. Fahrni, M. W. J. Prins, and L. J. van IJendoorn, *Lab Chip* **9**, 3413 (2009).
- ⁴¹A. Babataheri, M. Roper, M. Fermigier, and O. D. Roure, *J Fluid Mech* **678**, 5 (2011).
- ⁴²I. Javaitis and V. Zilgalve, *Adv Mat Res* **222**, 221 (2011).
- ⁴³J. L. Breidenich, M. C. Wei, G. V. Clatterbaugh, J. J. Benkoski, P. Y. Keng, and J. Pyun, *Soft Matter* **8**, 5334 (2012).
- ⁴⁴P. A. Sánchez, J. J. Cerda, V. Ballenegger, T. Sintès, O. Piro, and C. Holm, *Soft Matter* **7**, 1809 (2011).
- ⁴⁵S. Mørup, M. F. Hansen, and C. Frandsen, *Beilstein J Nanotechnol* **1**, 182 (2010).
- ⁴⁶J. D. Weeks, D. Chandler, and H. C. Andersen, *J Chem Phys* **54**, 5237 (1971).
- ⁴⁷Y. Sugita and Y. Okamoto, *Chem Phys Lett* **314**, 141 (1999).
- ⁴⁸H. J. Limbach, A. Arnold, B. A. Mann, and C. Holm, *Comp. Phys. Comm.* **174**, 704 (2006).
- ⁴⁹U. Micka and K. Kremer, *J Phys-Condens Mat* **8**, 9463 (1996).
- ⁵⁰U. Micka and K. Kremer, *Europhys Lett* **38**, 279 (1997).
- ⁵¹P. Bačová, P. Košován, F. Uhlík, J. Kuldová, Z. Limpouchová, and K. Procházka, *Eur. Phys. J. E Soft Matter* **35**, 1 (2012).
- ⁵²Z. Wang, C. Holm, and H. W. Müller, *Phys. Rev. E* **66**, 021405 (2002).
- ⁵³A. F. Pshenichnikov and V. V. Mekhonoshin, *J Magn Magn Mater* **213**, 357 (2000).
- ⁵⁴A. F. Pshenichnikov and V. V. Mekhonoshin, *Eur Phys J E* **6**, 399 (2001).
- ⁵⁵Z. Wang, C. Holm, and H. W. Müller, *J Chem Phys* **119**, 379 (2003).
- ⁵⁶C. Holm, A. Ivanov, S. Kantorovich, E. Pyanzina, and E. Reznikov, *J Phys-Condens Mat* **18**, S2737 (2006).
- ⁵⁷I. S. Jacobs and C. P. Bean, *Phys Rev* **100**, 1060 (1955).
- ⁵⁸C. Holm and J.-J. Weis, *Curr Opin Colloid Interface Sci* **10**, 133 (2005).
- ⁵⁹K. Šolc, *J Chem Phys* **55**, 335 (1971).
- ⁶⁰K. Alim and E. Frey, *Phys Rev Lett* **99**, 198102 (2007).
- ⁶¹BwGRiD (<http://www.bw-grid.de>), member of the German D-Grid initiative, funded by the Ministry for Education and Research (Bundesministerium fuer Bildung und Forschung) and the Ministry for Science, Research and Arts Baden-Wuerttemberg (Ministerium fuer Wissenschaft, Forschung und Kunst Baden-Wuerttemberg).
- ⁶²GRID-CSIC (<http://www.grid-csic.es>), Grid infrastructure for advanced research at the Spanish National Research Council, Ref. 200450E494.